Transformation Invariant Features Of Space Curves And Its Application In Classification Problems

D. Vignesh and T. Palanisamy*

Department of Mathematics Amrita, School of Physical Sciences Coimbatore, Amrita Vishwa Vidyapeetham, India

Corresponding author. E-mail: t_palanisamy@cb.amrita.edu

Received: July 21, 2023; Accepted: Oct. 09, 2023

The invariance property of curves under scaling, rotation and translation has been elaborately studied by research fraternity working on four-bar linkage mechanism. In fact, the authors detect that this invariance property will be useful in image classification problems. However, most of the existing works on four-bar linkage problems are associated with planar curves. Contrarily, the classification problems are based on the boundary space curves of the shapes of the images. Further, the strategy to study the invariance property adapted for the planar curve is not suitable for curves in space. Therefore, in our proposed work, the principal components of the sample points of the space curve are obtained, on which the atypical wavelet transform is performed for all the principal components. It is interesting to note that the desired relationship is found to be present in a specific ratio of atypical wavelet detailed coefficients of the points obtained by principal components. It is shown that this ratio, when included as a feature in classification problems enhances efficiency. In this study, we accomplish the classification of images by machine learning using the proposed feature along with the conventionally measured values.

Keywords: Space curves; Sample points; PCA; Atypical wavelet transform; Invariant feature vector; Classification; Machine learning; Measured values

http://dx.doi.org/10.6180/jase.202407_27(7).0013

1. Introduction

The proposed research article aims to explore the relationship between a space curve and its affine transformation. An entity used to establish this relationship is found to be a significant feature in classification problems. Numerous such investigations of the relationship between the curves are found useful in the study of four-bar linkage systems. Cartesian coordinates are employed in the case of planar four-bar linkages in studies of this issue, but spherical coordinates were used in the case of a four-bar linkage mechanism involving a space curve. All of these studies make an effort to unearth the hidden connections between members of the same family of curves that exhibit comparable geometric properties. After expressing the planar curve by its Fourier coefficients, different attempts have been made to create a feature vector that is invariant under scaling, translation and rotation.

For the convenience of readers, a few of these studies on the Fourier based four-bar connection mechanism are described here. Freudenstien and McGarva [1–3] have represented the coupler curve in four-bar mechanism using Fourier coefficients with the discussion of the geometric significance of harmonic terms. On the basis of normalised Fourier coefficients, McGarva [4] and Mullineux [5] obtained catalogues. Sun et al. [6] suggested a three-dimensional Fourier series for the analysis of coupler curves. Wu and Yue used the Fourier series to efficiently depict the coupler curve [7, 8]. The Fourier coefficients are appropriate for periodic curves; however, it is unavoid-

able to analyse open curves in numerous problems. This prompts Uesaka to propose the new Fourier description for open curves [9]. Despite this effort, Liu et al. [10] proved there are certain limitations [11] to using Fourier series on the open curves and hence wavelet coefficient descriptors of open non-periodic curves were obtained by them. There is also a study using wavelet coefficient descriptors for the space curves based on a spherical coordinate system [12].

It is significant to state that there are studies exclusively on the plane and space curves, independent of curves associated with linkage mechanisms using wavelet descriptors. In order to describe a plane closed curve that is invariant during scaling, translation and rotation, Hung et al. proposed the wavelet descriptor [13]. They also illustrated that the proposed descriptor can be used as a feature for pattern recognition. Tieng et al. [14] developed an algorithm for representing the space curves that are invariant under scaling, translation and rotation.

The proposed work attempts to study the invariance properties of curves in space represented by the Cartesian system. Liu et al. [10] in their attempt found the invariance property of the planar curves using the wavelet detailed coefficients. In fact, the ratio of the pair of wavelet detailed coefficients is found to be invariant. But it is to be noted that the computation of the ratio became possible by considering them as complex numbers [15]. Thus, the computation of the ratio used by Liu et al. [10] can never be accomplished for space curves. Therefore, in the proposed article, we extract the invariance property of the space curves using Principal Component Analysis (PCA). Thus, in this article, we propose a transformation invariant feature vector (TIFV) based on the wavelet coefficients of the sample points of the space curve. This paper is structured as follows for the remainder. Section 2. explains wavelets and principal component analysis in a concise manner. The proposed work is discussed in Section 3. The Illustrated examples of the proposed work are presented in Section 4. The classification problem studied in Section 5. The paper concludes with Section 6.

2. Review

2.1. Wavelet

In this section, we briefly discuss the development of wavelet decomposition techniques for real valued functions. The wavelet transform of a function $f(x)$ in $L^2(R)$ is the representation of it using a family of orthonormal bases of the form $\psi_{j,k}(x) = 2^{j/2}\psi(2^j x - k)$ obtained through translation and dilation of some $\psi(x)$ belongs to $L^2(R)$, known as the mother wavelet [16].

For this purpose, Mallat determined a set of properties that a sequence of embedded vector spaces $\{V_j\}_{j\in\mathbb{Z}}$ should have. With these properties the sequence becomes the Multiresolution Analysis (MRA) which in turn will yield a compactly supported wavelet system [17].

The above procedure is used in the next section to obtain the wavelet transform of the collection of sample points for the given parametric curve to describe the TIFV.

2.2. Principal component analysis

The choice of a new coordinate system for principal component analysis is made by rotating the existing system. A simpler and more concise representation of the relationship between the elements of the considered vectors is provided by the new axes, which represent the directions with the greatest degree of variability [18]. The wavelet transform of the sample points of the space curve will not result the required TIFV as we have done in planar curves and it has been found that this is due to rotation. To overcome this inability, we represent the sample points of a space curve by its principal components before obtaining the wavelet transform. We discuss the proposed TIFV for the space curve in the next section.

3. Transformation invariant feature vector

We consider a parametric curve

$$\mathbf{r}(t) = (x_1(t), x_2(t), x_3(t)) \in \mathbf{R^3}$$

Let

$$\mathbf{r}(t_i) = [x_1(t_i), x_2(t_i), x_3(t_i)]^T$$

for $i = 1, 2, \ldots, n$. where $n = 2^N$ be the sample points of the curve $\mathbf{r}(t)$ obtained by choosing values t_i of the parameter t.

Let us consider

$$P = \begin{bmatrix} \mathbf{r}(t_1) & \vdots & \mathbf{r}(t_2) & \vdots & \ldots & \vdots & \mathbf{r}(t_n) \end{bmatrix}$$

be the matrix consisting of sample points in columns.

Let the matrix A of size 3×3 be the change of basis matrix that represents the given n observations of three dimensions in the new basis which are the directions with maximum variability and provides a simpler and more parsimonious description of the relationship between the components of the considered vectors.

Let us denote

$$P^T A = Q = \begin{bmatrix} \mathbf{u}(t_1) & \vdots & \mathbf{u}(t_2) & \vdots & \ldots & \vdots & \mathbf{u}(t_n) \end{bmatrix}$$

where

$$\mathbf{u}(t_i) = [y_1(t_i), y_2(t_i), y_3(t_i)]^T$$

We obtain the componentwise wavelet transform of the $\{\mathbf{u}(t_i), i = 1, 2, \ldots, n\}$ after which we collect the triplets

of wavelet coefficients in order.
For this purpose we define

$$\mathbf{v_j} = (y_j(t_1), y_j(t_2), \ldots, y_j(t_n))^T$$

for $j = 1, 2, 3$. Then the k^{th} level wavelet transform $w_k(\mathbf{v_j})$ of $\mathbf{v_j}$, for $k = 1, 2, \ldots, N$ and $j = 1, 2, 3$ is

$$w_k(\mathbf{v_j}) = \left(a_{j(k,1)}, \ldots, a_{j\left(k,\frac{n}{2^k}\right)}, d_{j(k,1)}, \ldots, d_{j,\left(k,\frac{n}{2^k}\right)}, \ldots, d_{j(1,1)}, \ldots, d_{j\left(1,\frac{n}{2}\right)}\right)$$

In fact,

$$w_k(\mathbf{v_j}) = \sum_{m=1}^{\frac{n}{2^k}} \langle \mathbf{v_j}, \phi_{-k,m}\rangle \phi_{-k,m} + \sum_{l=1}^{k}\sum_{m=1}^{\frac{n}{2^k}} \langle \mathbf{v_j}, \psi_{-l,m}\rangle \psi_{-l,m}$$

where $\langle \mathbf{v_j}, \phi_{-k,m}\rangle = a_{j(k,m)}$ and $\langle \mathbf{v_j}, \psi_{-l,m}\rangle = d_{j(l,m)}$. Here ϕ and ψ will stand for the father and mother wavelet of the wavelet system we prefer for the proposed work.

We consider the following triplets of componentwise wavelet coefficients $\mathbf{w_{a_{k,p}}}$ which are taken in order. It is felt essential that the readers have to cognize the significance of this representation for the purpose of our proposed work. This can otherwise be thought of as an atypical wavelet transform of the collection of principal components $\{\mathbf{u} = \mathbf{u}(t_i)\ , i = 1, 2, \ldots, n\ \}$. Thus the k^{th} level wavelet transform $w_k(\mathbf{u})$ of the curve can be had as

$$w_k(\mathbf{u}) = \left(\mathbf{w_{a_{k,1}}}, \ldots, \mathbf{w_{a_{k,\frac{n}{2^k}}}}, \mathbf{w_{d_{k,1}}}, \mathbf{w_{d_{k,2}}}, \cdots, \mathbf{w_{d_{k,\frac{n}{2^k}}}}, \ldots, \mathbf{w_{d_{1,1}}}, \mathbf{w_{d_{1,2}}}, \ldots, \mathbf{w_{d_{k,\frac{n}{2}}}}\right)$$

where $\mathbf{w_{a_{k,p}}} = (a_{1(k,p)}, a_{2(k,p)}, a_{3(k,p)})^T$ for $p = 1, 2, \ldots, \frac{n}{2^k}$, and
$\mathbf{w_{d_{q,p}}} = (d_{1(q,p)}, d_{2(q,p)}, d_{2(q,p)})^T$, where $q = 1, 2, \ldots, N$ and $p = 1, 2, \ldots, \frac{n}{2^q}$ for every q.

Nevertheless, the fact that we use the unconventional wavelet transform for our study, it is interesting to note that it can also be represented by using the Nth level wavelet transform matrix as

$$(W_N Q^T)^T = \begin{bmatrix} W_N(\mathbf{v_1}) & \vdots & W_N(\mathbf{v_2}) & \vdots & W_N(\mathbf{v_3}) \end{bmatrix}$$
$$= \begin{bmatrix} a_{1(N,1)} & d_{1(N,1)} & \cdots & d_{1(1,\frac{n}{2})} \\ a_{2(N,1)} & d_{2(N,1)} & \cdots & d_{2(1,\frac{n}{2})} \\ a_{3(N,1)} & d_{3(N,1)} & \cdots & d_{3(1,\frac{n}{2})} \end{bmatrix}$$
$$= \begin{bmatrix} \mathbf{w_{a_{N,1}}} & \vdots & \mathbf{w_{d_{N,1}}} & \vdots & \cdots & \vdots & \mathbf{w_{d_{1,\frac{n}{2}}}} \end{bmatrix}$$

It is understood to be essential to explore the intrinsic relationship between the sample points of the actual curve and the transformed sample points using scaling, rotation and translation to obtain the proposed TIFV of the space curve. In fact, the transformed sample points can be represented by $\tilde{P} = (S \circ R_\theta \circ M)P$, where $S = \begin{bmatrix} s & 0 & 0 \\ 0 & s & 0 \\ 0 & 0 & s \end{bmatrix}$ represents the scaling,

$$R_z(\alpha)R_y(\beta)R_x(\gamma) = \begin{bmatrix} \cos\alpha\cos\beta & \cos\alpha\sin\beta\sin\gamma - \sin\alpha\cos\gamma & \cos\alpha\sin\beta\cos\gamma + \sin\alpha\sin\gamma \\ \sin\alpha\cos\beta & \sin\alpha\sin\beta\sin\gamma + \cos\alpha\cos\gamma & \sin\alpha\sin\beta\cos\gamma - \cos\alpha\sin\gamma \\ -\sin\beta & \cos\beta\sin\gamma & \cos\beta\cos\gamma \end{bmatrix}$$

represents the rotation whose yaw, pitch and roll angles are α, β, γ about axis z, y, x and $M = \begin{bmatrix} t_x & t_x & \cdots & t_x \\ t_y & t_y & \cdots & t_y \\ t_z & t_z & \cdots & t_z \end{bmatrix}^T_{3\times n}$ represents the translation of (x_i, y_i, z_i) to $(x_i + t_x, y_i + t_y, z_i + t_z)$ for $i = 1, 2, \ldots, n$.
Further we mean $S \circ P = SP$, $R_\theta \circ P = R_\theta P$ and $M \circ P = P + M^T$.
Now we consider the wavelet transform of principal component of the transformed sample points

$$\begin{aligned} & W_N\tilde{Q}^T = W_N(\tilde{P}^T\tilde{A}) \\ &= W_N(SR_\theta P + M^T)^T\tilde{A} \\ &= W_N((SR_\theta P)^T\tilde{A} + M\tilde{A}) \\ &= W_N(P^T(SR_\theta)^T R_\theta A + M\tilde{A}) \\ &= W_N(P^T S^T R_\theta^T R_\theta A + M\tilde{A}) \\ &= W_N P^T S A + W_N M\tilde{A}. \end{aligned}$$

Let us denote the resulting coefficients of atypical wavelet transform of the transformed sample points as

$$(W_N\tilde{Q}^T)^T = \begin{bmatrix} \tilde{a}_{1(N,1)} & \tilde{d}_{1(N,1)} & \cdots & \tilde{d}_{1(1,\frac{n}{2})} \\ \tilde{a}_{2(N,1)} & \tilde{d}_{2(N,1)} & \cdots & \tilde{d}_{2(1,\frac{n}{2})} \\ \tilde{a}_{3(N,1)} & \tilde{d}_{3(N,1)} & \cdots & \tilde{d}_{3(1,\frac{n}{2})} \end{bmatrix}$$
$$= \begin{bmatrix} \tilde{\mathbf{w}}_{\mathbf{a_{N,1}}} & \vdots & \tilde{\mathbf{w}}_{\mathbf{d_{N,1}}} & \vdots & \cdots & \vdots & \tilde{\mathbf{w}}_{\mathbf{d_{1,\frac{n}{2}}}} \end{bmatrix}$$

It is easy to understand that the first row of $W_N\tilde{Q}^T$ has the influence of scaling and translation but the remaining rows have the influence of scaling only. This became possible due to the rotation invariance property under the principal component representation of vectors and the shifting invariance property under the wavelet transform. By denoting the normalized wavelet detailed vectors $\mathbf{f} = \frac{\mathbf{w_{d_{q,p}}}}{\mathbf{w_{d_{N,1}}}}$ and $\tilde{\mathbf{f}} = \frac{\tilde{\mathbf{w}}_{\mathbf{d_{q,p}}}}{\tilde{\mathbf{w}}_{\mathbf{d_{N,1}}}}$ where $q = 1, 2, \ldots, N$ and $p = 1, 2, \ldots, \frac{n}{2^q}$ for every q, we can easily verify that $\mathbf{f} = \tilde{\mathbf{f}}$. Thus our ef-

fort to capture the intrinsic relation between the sample points of the actual curve and transformed curve is found to be obtained through the above said ratio of the vectors of wavelet detailed coefficients. Therefore, we justified that the vector $\mathbf{f} = \tilde{\mathbf{f}}$ can be called as TIFV of any space curve. The proposed TIFV of various curves are illustrated in next section.

4. Results and discussion

We present the computation of the proposed TIFV of some of the sample curves in this section. For this purpose, we consider the sample points of the actual curve and their transformations. The parametric curves $x(t) = \cos(t)$, $y(t) = \sin(t)$, $z(t) = t$ and $x(t) = t$, $y(t) = t^2$, $z(t) = t^3$ are considered for the study to justify the invariance property of the computed parameter for various types of curves. The actual, scaled, rotated and translated versions of the curves considered above are depicted in Figs. 1 and 2 respectively. We have used Haar wavelet and Daubechies wavelet of fourth order for the computation [19, 20]. We take 64 equally spaced sample points. We have implemented the computations using MATLAB R2013a. We have carried out all six levels of wavelet transform for both sets of points obtained by PCA. Using each of the two wavelets, the necessary parameters for all the curves under consideration are found. Despite these facts, the wavelet detailed coefficients of the points obtained by PCA of $x(t) = \cos(t)$, $y(t) = \sin(t)$, $z(t) = t$ by Haar, and $x(t) = t$, $y(t) = t^2$, $z(t) = t^3$ by Daubechies 4. only are presented in Tables 1 and 2 respectively. Further, it is to be noted that the computational details of the last three levels only are given in the tables.

We briefly discuss the computation of the proposed TIFV for $x(t) = \cos(t)$, $y(t) = \sin(t)$, $z(t) = t$ by using Haar. We take 64 equally spaced sample points of $x(t) = \cos(t)$, $y(t) = \sin(t)$, $z(t) = t$, $0 \leq t \leq 63$. We also obtained the scaled, rotated and translated points of the parametric curve using $s = 2$, $\alpha = \beta = \gamma = 30^\circ$, $t_x = 2$, $t_y = 3$ and $t_z = 4$. We obtain the atypical wavelet detailed coefficients of the principal components of the sample points. In our effort to identify the relationship between both sets of sample points, nothing is found to be evidently extracted from either the sample points or from their wavelet coefficients. This observation is not as devastating to our plans as it appears because it turns out that the proposed TIFV leads to the desired results. This TIFV is obtained by dividing all the wavelet detailed coefficients by the last level wavelet detailed coefficient [10] [15] of both the sets of actual and transformed principal components. It is observed that the vectors $\mathbf{f}$ and $\tilde{\mathbf{f}}$ are the same. Thus, these vectors capture the intrinsic relationship between both the sets of actual and transformed sample points and hence the resulting vector $\mathbf{f} = \tilde{\mathbf{f}}$ can be defined as the TIFV of a space curve.

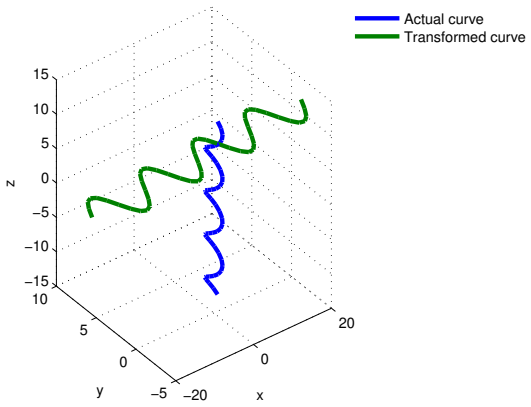

Fig. 1. $x(t) = \cos(t)$, $y(t) = \sin(t)$, $z(t) = t$.

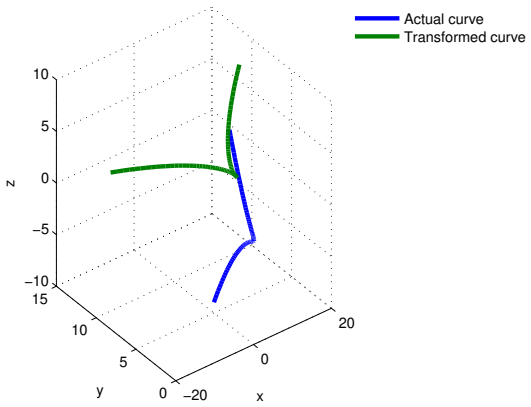

Fig. 2. $x(t) = t$, $y(t) = t^2$,$z(t) = t^3$.

5. Strawberry image classification using TIFV

In this section, we study the influence of TIFV in the classification of strawberry shapes shown in Fig. 3.

For the purpose of classification, we generated a data set of 61 images of each of the nine types of strawberries. The classification is made using machine learning techniques based on the random forest method and Support Vector Machine (SVM) [21, 22]. We briefly present the preprocessing for the required image to be studied. For this purpose, we use Python programming to extract the

Table 1. TIFV using Haar.

No.	$\mathbf{w_{d(q,p)}}$	$\tilde{\mathbf{w}}_{\mathbf{d(q,p)}}$	$\mathbf{f}/\tilde{\mathbf{f}}$
q=6,p=1	(-45.2564, 0.20782, 0.57792)	(-90.5085, 0.41529, 1.15589)	(1.00000, 1.00000, 1.00000)
q=5,p=1	(-45.2564, -0.20782, 0.57792)	(-90.5085, -0.41596, 1.15567)	(0.99999, -1.00159, 0.99980)
q=5,p=2	(-15.9993, 0.54093, -0.29345)	(-31.9971, 1.08198, -0.58658)	(0.35353, 2.60534, -0.50747)
q=4,p=1	(-16.0002, -0.59097, 0.04683)	(-31.9988, -1.18193, 0.09334)	(0.35354, -2.84601, 0.08075)
q=4,p=2	(-16.0002, 0.59097, 0.04683)	(-31.9988, 1.18187, 0.09398)	(0.35354, 2.84588, 0.08131)
q=4,p=3	(-15.9993, -0.54093, -0.29345)	(-31.9971, -1.08165, -0.58717)	(0.35353, -2.60454, -0.50798)
q=4,p=4	(-5.65978, -0.33037, 1.15971)	(-11.3190, -0.66136, 2.31913)	(0.12506, -1.59253, 2.00635)

Table 2. TIFV using Daubechies 4.

No.	$\mathbf{w_{d(q,p)}}$	$\tilde{\mathbf{w}}_{\mathbf{d(q,p)}}$	$\mathbf{f}/\tilde{\mathbf{f}}$
q=6,p=1	(225559, 1416.94, -2.66276)	(451096, 2833.76, -5.32532)	(1.00000, 1.00000, 1.00000)
q=5,p=1	(-145768, 493.263, 10.2149)	(-291522, 986.480, 20.4291)	(-0.64625, 0.34812, -3.83622)
q=5,p=2	(421936, -352.222, -1.72989)	(843833, -704.412, -3.45965)	(1.87063, -0.24858, 0.64966)
q=4,p=1	(-13491.1, 255.669, 3.53239)	(-26980.9, 511.315, 7.06453)	(-0.05981, 0.18044, -1.32659)
q=4,p=2	(22834.7, -15.6322, -1.84907)	(45667.3, -31.2630, -3.69800)	(0.10124, -0.01103, 0.69442)
q=4,p=3	(-3114.37, -15.2144, -0.39587)	(-6228.59, -30.4281, -0.79174)	(-0.01381, -0.01074, 0.14867)
q=4,p=4	(214463, -350.081, 6.28329)	(428905, -700.131, 12.5661)	(0.95081, -0.24707, -2.35969)

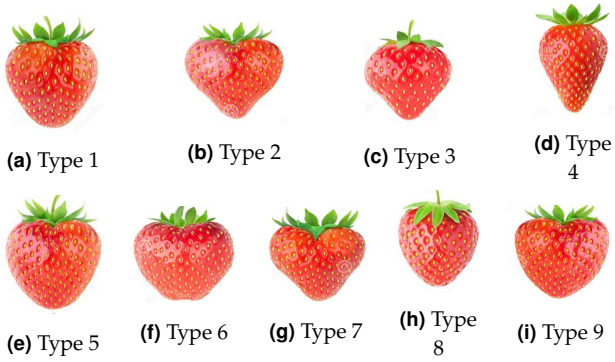

Fig. 3. Fruit images of nine shapes

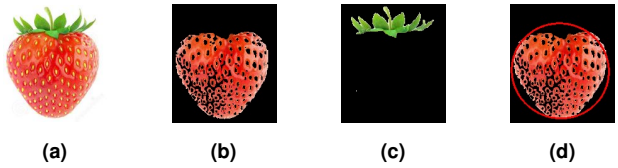

Fig. 4. (a) Original colour image (b) Fruit body region (c) Calyx region (d) Ellipse approximation of fruit body region

feature parameters for the above said images. In fact, Red, Green and Blue (RGB) colour space is used to extract the fruit portion from each strawberry image by removing the calyx of the fruit as shown in Fig. 4 [23]. In the next step, the conventional measured values (MV) along with the proposed TIFV using the boundary pixels of fruit portions are computed. We have used Google Colab for machine learning algorithms. It primarily offers CPU computing, GPU support and substantial memory. It also offers cloud-based storage for our datasets, code and experiment results, ensuring accessibility and reproducibility. Google Colab supports Python, making it compatible with popular machine-learning libraries like Scikit-learn and Tensor Flow. The performance of the proposed classification study involving TIFV is compared with that of the existing classification study using measured values of two dimension images of strawberries along with ellipse similarity index, elliptic fourier descriptors and chain code subtraction [24]. In fact, the proposed work uses features of MV of the two dimension images along with TIFV of the three dimension images of strawberries. The MV's included length of the contour line, area, major axis of the approximate ellipse or fruit length, minor axis of the approximate ellipse or fruit width and ratio of fruit length/width. The proposed method of obtaining the TIFV of the space curve discussed in Section 3. is used in the classification study of 3D pixels of strawberry images. It is interesting to observe that the inclusion of TIFV along with the rest of the features enhances the classification efficiency.

5.1. Classification by Random forest method

We use the sklearn module for training our Random Forest Model, specifically the Random Forest Classifier function. Hyper-parameter tuning and cross-validation strategies are expected to significantly impact model performance [21]. We used 100 binary decision trees in this study. The random forest approach considers the different types of

strawberry shapes pairwise resulting in 9C2 = 36 pairs for the study [24]. For each image pair, we generate the subsets from the complete dataset for the two images that are considered for comparison. Features and labels are combined for the two images to form the training set. We carry out two classification studies of strawberry images, one using MVs and the other using TIFV along with MVs. The performance of the classification was measured using the weighted recall ratio. Recall ratios equal to or greater than 0.8, 0.7, 0.6 and less than 0.6 were classified as great, good, fair and requiring re-work respectively. The first study, which uses MVs only revealed that 15 out of the 36 pairs achieved a recall ratio of ≥ 0.6 as shown in Fig. 5, the other study using MVs and TIFVs shows that all 36 pairs achieved a recall ratio of ≥ 0.6 as shown in Fig. 6. The comparison of these two studies reveals that the TIFV proposed in this article improves the classification performance of the random forest method. We also used cross-validation technique to ensure the performance of the classification considering the combination of MVs along with TIFV.

5.2. Classification by Support Vector Machine

We use the sklearn module for training our SVM, specifically the Support Vector Classifier (SVC) function. The SVC is employed as the base classifier within the binary relevance transformation. The linear kernel parameter associated with the SVC is used in our study. Feature scaling is used in our study to help the SVM algorithm converge faster and ensure that the decision boundary is not biased towards features with larger numeric ranges. We also used the multi-label binarizer which simplifies multi-label classification tasks by converting them into multiple binary classification sub tasks, making it easier for SVM to learn and make predictions. In fact, we use the tensor flow that provides GPU acceleration for certain operations and significantly speeds up computations. To ensure the reproducibility of data splitting, the random state parameter is set to 42 when splitting the data into training and testing sets [22]. We then proceeded with the algorithm by considering MVs in one case and TIFVs in the other. In both cases, labelled data sets were provided as input. In our study, we used a linear kernel for classification. In fact, 80% of 549 images are used as training set and 20% are taken for test. The SVM algorithm found an optimal hyperplane that separates the classes using the training set and classifies the data of the test set [22]. The results of the SVM algorithm show that the classification model including TIFV performs much better with 100% accuracy compared to the model just with MVs which has 51.82% accuracy. Of course, the studies are also carried out using polynomial kernel and RBF kernel, which result in the same accuracy level of classification. Thus, this classification study shows clearly that the inclusion of TIFV is proposed in Section 3. improves the the classification performance.

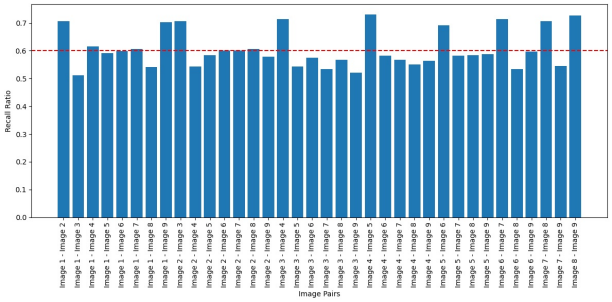

Fig. 5. The results of classification by MVs

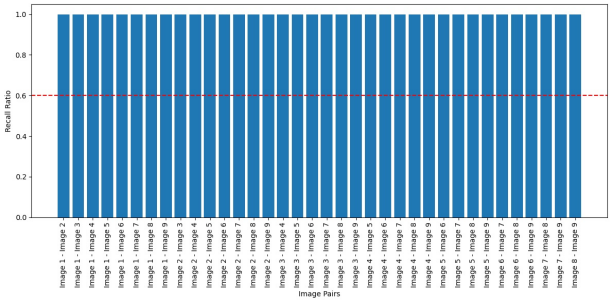

Fig. 6. The results of classification by MVs+TIFV

6. Conclusion

The relationship between the sample points of a space curve and scaled, rotated and translated sample points is studied in our work. It is interesting to state that the proposed TIFV is useful as a feature for the study related to image classification. However, a plethora of attempts have been made on planar curves using Fourier and wavelet transforms. It is observed that the strategy adapted for the planar curve is not suitable for the curves in space. Therefore, we made our effort to study the relationship using the principal components of the sample points, we then obtained the atypical wavelet coefficients instead of actual sample points. The required relationship is not evident even with the wavelet coefficients of the principal components. However, we could extract these intrinsic relationships by a specific ratio of the wavelet detailed coefficients of the principal components. This study is accomplished by using atypical orthogonal wavelet coefficients for both sets of principal components of the sample points. In fact, we have established these relationships by mathematical analysis. Our results are illustrated with a few continuous space curves.

We have used various orthogonal wavelets to perform an atypical wavelet transform. The results were found to be independent of the wavelets used. In our work, we have also studied the performance of the classification using TIFV as a feature of the well known nine strawberry images. We have considered two classification models, one using features without TIFV and the other with TIFV. The study was performed using random forest and SVM algorithms. It is found in both cases that the results of the classification are much improved when TIFV is included. Thus, the proposed TIFV is very useful for problems of classification.

Acknowledgment

The authors wish to acknowledge the valuable comments and suggestions of the anonymous reviewers that improved the quality of the manuscript.

References

[1] F. Freudenstein, (1959) *"Harmonic analysis of crank-and-rocker mechanisms with application"* **Journal of Applied Mechanics *26***: 673–675.

[2] J. McGarva and G. Mullineux, (1992) *"A new methodology for rapid synthesis of function generators"* **Proceedings of the Institution of Mechanical Engineers, Part C: Journal of Mechanical Engineering Science *206***: 391–398. DOI: 10.1243/PIME_PROC_1992_206_146_02.

[3] J. McGarva and G. Mullineux, (1993) *"Harmonic representation of closed curves"* **Applied Mathematical Modelling *17***: 213–218. DOI: 10.1016/0307-904x(93)90109-t.

[4] J. R. McGarva, (1994) *"Rapid search and selection of path generating mechanisms from a library"* **Mechanism and machine theory *29***: 223–235. DOI: 10.1016/0094-114x(94)90032-9.

[5] G. Mullineux, (2011) *"Atlas of spherical four-bar mechanisms"* **Mechanism and machine theory *46***: 1811–1823. DOI: 10.1016/j.mechmachtheory.2011.06.001.

[6] J. Sun, J. Chu, and B. Sun, (2012) *"A unified model of harmonic characteristic parameter method for dimensional synthesis of linkage mechanism"* **Applied Mathematical Modelling *36***: 6001–6010. DOI: 10.1016/j.apm.2012.01.052.

[7] J. Wu, Q. Ge, and F. Gao, (2009) *"An efficient method for synthesizing crank-rocker mechanisms for generating low harmonic curves"* **International Design Engineering Technical Conferences and Computers and Information in Engineering Conference *49040***: 531–538. DOI: 10.1115/DETC2009-87140.

[8] C. Yue, H.-J. Su, and Q. J. Ge, (2012) *"A hybrid computer-aided linkage design system for tracing open and closed planar curves"* **Computer-Aided Design *44***: 1141–1150. DOI: 10.1016/j.cad.2012.06.004.

[9] Y. Uesaka, (1984) *"A new Fourier descriptor applicable to open curves"* **Electronics and Communications in Japan (Part I: Communications) *67***: 1–10. DOI: 10.1002/ecja.4400670802.

[10] W. Liu, J. Sun, B. Zhang, and J. Chu, (2018) *"Wavelet feature parameters representations of open planar curves"* **Applied Mathematical Modelling *57***: 614–624. DOI: 10.1016/j.apm.2017.05.035.

[11] S. Anusha, A. Sriram, and T. Palanisamy, (2016) *"A Comparative Study on Decomposition of Test Signals Using Variational Mode Decomposition and Wavelets"* **International Journal on Electrical Engineering and Informatics *8***: 886. DOI: 10.15676/ijeei.2016.8.4.13.

[12] J. Sun, W. Liu, and J. Chu, (2018) *"Synthesis of spherical four-bar linkage for open path generation using wavelet feature parameters"* **Mechanism and Machine Theory *128***: 33–46. DOI: 10.1016/j.mechmachtheory.2018.05.008.

[13] K.-C. Hung, T.-K. Truong, J.-H. Jeng, and J.-T. Yao. "Uniqueness wavelet descriptor for plane closed curves". In: ***1***. IEEE, 1997, 294–297. DOI: 10.1109/PACRIM.1997.619958.

[14] Q. M. Tieng, W. W. Boles, and M. Deriche. "Space curve recognition based on the wavelet transform and string-matching techniques". In: **2**. IEEE, 1995, 643–646. DOI: 10.1109/ICIP.1995.537561.

[15] D. Vignesh and T. Palanisamy, (2022) *"Invariance Of Geometry Of Planar Curves Using Atypical Wavelet Coefficients"* **Journal of Applied Science and Engineering *26***(5): 731–737. DOI: 10.6180/jase.202305_26(5).0014.

[16] M. W. Frazier. *An introduction to wavelets through linear algebra*. Springer Science & Business Media, 2006.

[17] S. G. Mallat, (1989) *"Multiresolution approximations and wavelet orthonormal bases of $L^2(\mathbb{R})$"* **Transactions of the American mathematical society *315***(1): 69–87.

[18] J. Ma and Y. Yuan, (2019) *"Dimension reduction of image deep feature using PCA"* **Journal of Visual Communication and Image Representation *63***: 102578. DOI: 10.1016/j.jvcir.2019.102578.

[19] I. Daubechies, (2001) *"Ten lectures on wavelets. Philadelphia: SIAM; 1992"* **Google Scholar Google Scholar Digital Library Digital Library**: DOI: 10.1137/1.9781611970104.

[20] R. Gokul, A. Nirmal, G. Dinesh Kumar, S. Karthic, and T. Palanisamy, (2020) *"A Combined Wavelet and Variational Mode Decomposition Approach for Denoising Texture Images"* **International Conference on Computer Vision and Image Processing**: 50–62. DOI: https://doi.org/10.1007/978-981-16-1092-9_5.

[21] L. Breiman, (2001) *"Random forests"* **Machine learning *45***: 5–32. DOI: 10.1023/A:1010933404324.

[22] U. S. Bist and N. Singh, (2022) *"Analysis of recent advancements in support vector machine"* **Concurrency and Computation: Practice and Experience *34***(25): e7270. DOI: https://doi.org/10.1002/cpe.7270.

[23] L. M. Oo and N. Z. Aung, (2018) *"A simple and efficient method for automatic strawberry shape and size estimation and classification"* **Biosystems engineering *170***: 96–107. DOI: 10.1016/j.biosystemseng.2018.04.004.

[24] T. Ishikawa, A. Hayashi, S. Nagamatsu, Y. Kyutoku, I. Dan, T. Wada, K. Oku, Y. Saeki, T. Uto, T. Tanabata, et al., (2018) *"Classification of strawberry fruit shape by machine learning"* **The International Archives of the Photogrammetry, Remote Sensing and Spatial Information Sciences *42***: 463–470. DOI: 10.5194/isprs-archives-XLII-2-463-2018.